OPTIMISATION OF MULTISTABLE HELICAL STRUCTURES USING AFP MANUFACTURING

Robert Telford[1] and Paul M. Weaver[2]

[1] Varicomp, Bernal Institute, University of Limerick, Co. Limerick Ireland, robert.telford@ul.ie, www.ul.ie
[2] Varicomp, Bernal Institute, University of Limerick, Co. Limerick Ireland, paul.weaver@ul.ie, www.ul.ie

Keywords: Twist Morphing, Helix, Perversion, AFP

ABSTRACT

We are currently in a remarkable period of spaceflight, with an ever-growing number of private companies and governments launching increasingly frequent and ambitious missions. Aggressive development of new technologies has led to a reduction in launch costs while improving mission capabilities. One such technology that can benefit space missions is shape changing and deployable structures (herein referred to as morphing structures). By undergoing large changes in shape, it is possible to package deployable structures in a small volume, reducing the size and weight of launch structures while also adding multi-functionality.

The morphing helix is one such structure which offers exceptional twist and length shape changing capabilities, in a lightweight, simple and highly tuneable system. As such, it is an ideal morphing solution for aerospace applications. This work aims to improve the viability of morphing helices in two areas. Firstly, the morphing configurations possible are increased by incorporating perversions, which locally invert the twist angle of the helix. Secondly, advanced manufacturing techniques (automated fibre placement) is explored as a means to quickly and accurately manufacture morphing components.

Initial findings from a manufactured demonstrator showed that high strains can develop by reversing twist direction, which limited the formation of a perversion. A finite element model was developed to investigate this finding. It was found that membrane strains develop within the perversion region, which may require modification to theoretical approaches predicting perversions in morphing helices.

1 INTRODUCTION

Morphing structures are capable of undergoing large, controlled and seamless shape changes in order to optimise the functionality for different requirements [1, 2]. Potential beneficiaries of such technology include the aeronautical and wind energy industries, that use morphing wings or blades to eliminate hinged aerodynamic surfaces. This leads to an increase in aerodynamic efficiency due to elimination of aerodynamic gaps, as well as a loss in weight due to removal of heavy and complex actuation systems. Further weight reductions are also possible through active load alleviation. As a result, aircraft benefit from a reduction in fuel consumption and carbon emissions, while wind turbines increase energy harvesting capabilities [3, 4]. Deployable structures also provide substantial benefits to spacecraft. Due to payload volume/weight constraints imposed by the launch vehicles, structures that can be stowed for launch and deployed in space are particularly advantageous [5]. Enhancing the shape changing capabilities of a structure while minimising weight is therefore of key industrial interest.

Maximising the potential of morphing structures is currently hindered by the opposing requirements of a flexible surface capable of large deformations (enabling morphing), structural rigidity (reducing deformation under in-service loads) and low weight (to achieve efficiency goals) [6-8]. Composite materials can provide solutions to these challenges. Firstly, by exploiting anisotropic material properties and pre-stress of fibre-matrix composites, novel morphing structures with large deformations and tailored strain energy landscapes become possible. Secondly, the high strength-to-weight ratio of composite materials allows for strong yet lightweight structures. When combined, these properties enable lightweight yet stiff structures that can morph through careful control of their flexural stiffness. Finally, by exploiting fibre steering and precise control of Automated Fibre Placement (AFP), it is

possible to develop a new range of viable morphing structures featuring variable stiffness and complex geometries. AFP is used in this work as an enabling technology to manufacture a helix demonstrator featuring a perversion. Firstly, the in-situ material processing possible with AFP eliminates costly autoclave processing, while also reducing manufacturing times and complexity. In addition, the precise control over fibre orientation improves the tailoring of the strain energy landscape. Combined with fibre steering capabilities, AFP expands the design space of morphing composites to produce novel, unique and optimised structures.

A morphing helix is an example of a deployable morphing structure that can be optimised further by AFP manufacturing. The structure consists of two curved composite strips, which are subsequently flattened and connected by rigid spokes. This process introduces pre-stress, which can be tailored (by means of changing the spoke length, the strip's initial curvature or its stacking sequence) to provide the desired multistable response (see Figure 1(a-c)**)**.

It has recently been reported [9] that increasing the length of a multistable helix beyond a critical value can result in a *perversion* being introduced. This perversion reverses the direction of twist of the structure, as shown in see Figure 1(d), and creates new opportunities for morphing helices in morphing structures.

This work aims to observe experimentally the existence of a perversion in a multistable helix. AFP was used to manufacture the strips by laying Carbon Fibre Reinforced Plastic (CFRP) tape circumferentially onto a cylindrical mandrel. Once manufactured, the strip was cut into two 957 mm lengths and assembled into a helix. Ten equally spaced spokes were used to connect the strips. Two multistable helical shapes were immediately obtainable, with a ± 45° angle of twist. It was not possible to introduce any perversions in this configuration. However, upon removal of a spoke it was possible to introduce a stable perversion and reverse the direction of twist. This finding was analysed by using finite element models to monitor the strain energy developed during the formation of a perversion.

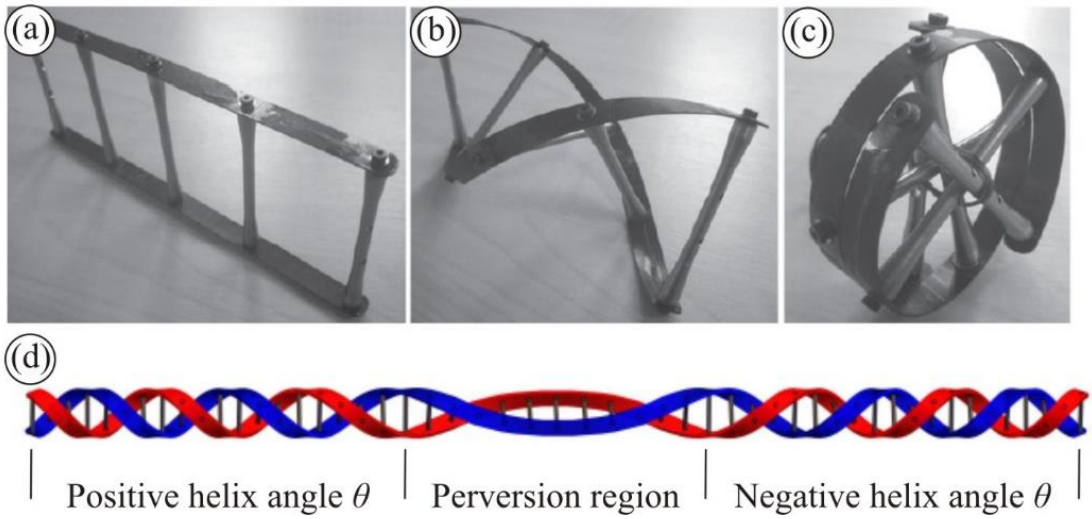

Figure 1: Shape configurations obtainable with morphing helices, including (a) straight 'ladder' configuration; (b) helix configuration; (c) stowed 'coiled' configuration; and (d) helix with perversion (reproduced without permission from [9]).

2 THE MORPHING HELIX

The configuration of the morphing is shown in Fig 2. The principle characteristic used to describe the shape of the structure is the helix angle, θ. This can be controlled by varying the material properties or stacking sequence of the composite strips, changing the manufactured radius of curvature of the structure, or changing the spoke length (H). For a comprehensive description of this behaviour, including an analytical model based on the minimisation of potential energy, the reader is referred to [4].

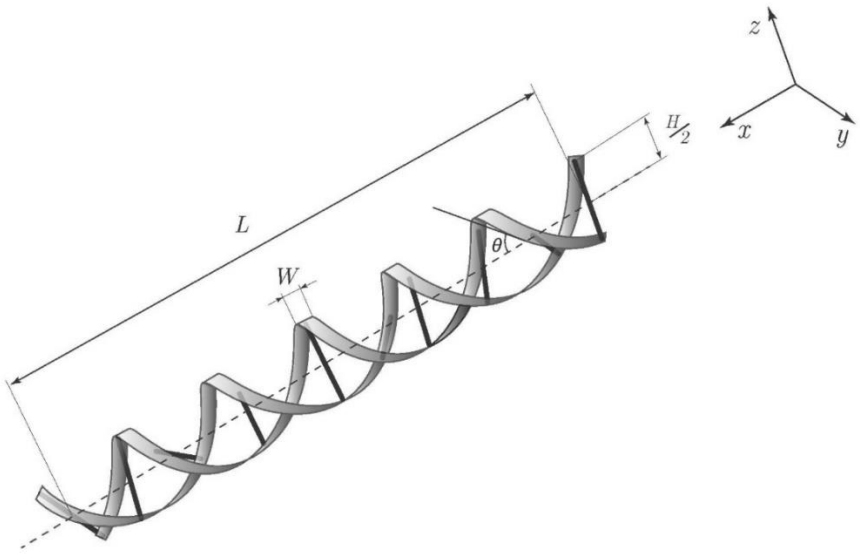

Fig 2: Description of the morphing helix.

It is important to note that the analytical model developed assumes that membrane strains are negligible, and thus are ignored (*i.e.* that no mid-plane stretching occurs in the flanges). Lessinnes and Goriely [9] subsequently developed a model to predict the existence and characteristics of a perversion. As before, this model neglects membrane strains.

2.1 Manufactured demonstrator

The strips of the demonstrator were manufactured by AFP, laying carbon fibre/PEEK prepreg tape onto a rotating cylindrical mandrel of 6" (152.4 mm) diameter. The AFP system comprises a Kuka KR240 automated robot coupled to an AFPT thermoplastic tape laying head. The processing of the material is handled in-situ, with a 3 kW laser being used to heat the thermoplastic material. The laser is autonomously controlled on a closed loop. The material used was Suprem IM7/PEEK thermoplastic prepreg tape. The tape width was measured following manufacture, and found to be 13 mm. The properties of the tape are given in Table 1.

E_{11} (GPa)	E_{22} (GPa)	G_{12} (GPa)	υ_{12}	υ_{21}	Nominal thickness (mm)
147.6	8.94	8.94	0.3*	0.021*	0.11*

Table 1: Experimentally measured material properties Note: * denotes estimated values.

A single strip was manufactured by winding through four complete revolutions of the tool, requiring an offset of one tape width per revolution. This strip was later split into two to form the top and bottom flanges, resulting in a flange length of 957 mm. Finally, a $[0_4]$ lay-up was used. Once the tool was mounted, the entire process of manufacturing the strips took under 30 minutes. This is a significant saving in time compared to traditional autoclave processing of thermoset materials, which would require cutting and lay-up of pre-preg material, bagging over a cylindrical tool and processing in an autoclave. This process would likely take a full day of manufacturing.

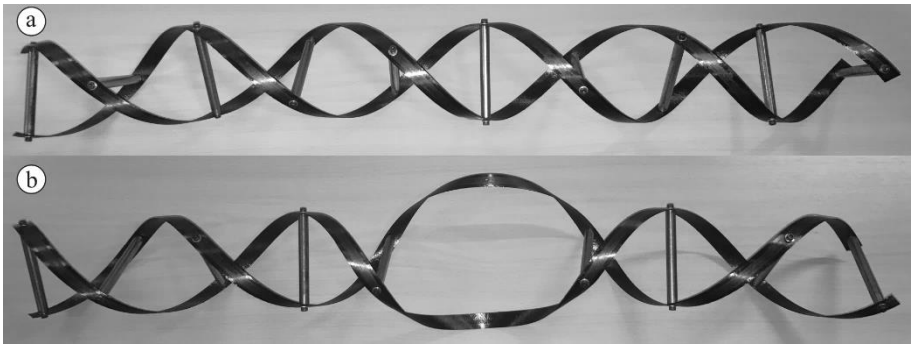

Figure 3: Manufactured demonstrator, showing (a) the helix configuration and (b) the perversion configuration, featuring a twist reversal. Note the missing spoke in the perversion region.

With the strips manufactured, the morphing helix could then be assembled by connecting the two strips. Ten steel spokes of length H = 76.2 mm were used to act as rigid links between to the two flanges. These spokes were threaded to accept an M3 sized bolt, which was used to connect the flanges to the spoke.

Once manufactured, the structure obtained the configuration shown in Figure 3(a), with a helical angle θ of 45°. Applying a twisting motion to the end of the structure resulted in the structure obtaining a helix angle of opposite orientation (*i.e.* θ = -45°). The existence of a shape perversion was then explored by trying to locally reverse the twist orientation of the structure. The centremost spoke was held rigid, and an opposing twist was applied to the end of the structure. It was not possible to introduce a perversion in this manner, as the structure was noticeably highly stressed, with cracking sounds indicating the onset of failure. To reduce the high stresses developed, the centremost spoke was removed, removing the constraint of a constant distance between the flanges. This modification reduced the stresses developed such that the perversion could now be formed, as shown in Figure 3(b).

3 FINITE ELEMENT MODELLING

Based on the experimental observations described in Section 2, a Finite Element (FE) model was developed to predict the helix shapes observed and to provide insight into the strains developed while introducing a perversion. The model was created and run using ABAQUS; a commercially available FE software.

Two separate models were developed. Firstly, the deformation of the complete structure (including both flanges) was modelled. This gave a qualitative look at the shapes predicted by modelling. A modified version of this model was then used for an in-depth investigation of the flexural and membrane strains developed during the formation of the perversion region.

Newton-Raphson iterative methods were used in both models, along with large-displacements formulation (*NLGEOM*) to account for geometric non-linearity. The thin nature of the strips allowed for the use of shell elements (type S4R). Due to the potential for high stresses being formed in the location of the perversions, a denser mesh than that presented by Lachenal et al. [4] was used. The mesh featured 8 elements across the width (1.625 mm) and 639 elements along the length (1.5 mm) of the strips. The material properties used were as in Table 1.

3.1 Qualitative FE model to capture helix shapes

Modelling the complete structure involved two separate analyses. Firstly, the process of flattening the flanges to introduce the pre-stress was simulated by unravelling a coiled strip. As per the manufactured helix, the strips were modelled as being circumferentially wound through two rotations over a cylinder of radius R_1 = 76.2 mm, with an axial displacement of 14 mm per revolution. The deformation of the structure was controlled by using ten Reference Points (RPs) which are linked to the flanges using beam connectors. The locations of the spokes corresponded to those of the spokes in the manufactured demonstrator. The RPs were then restricted, as per Figure 4. Rotational boundary conditions were then applied to the RPs to unravel the strips into a flat configuration.

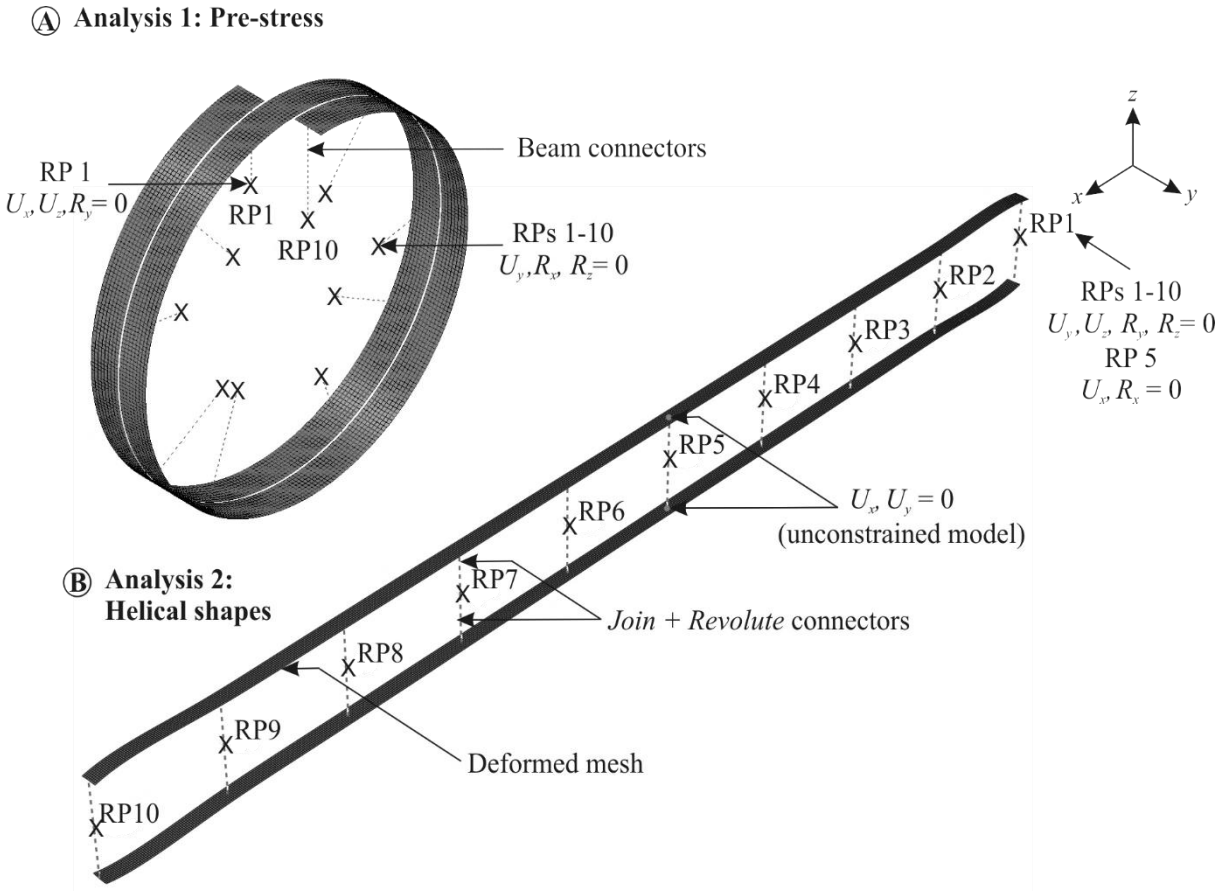

Figure 4: Numerical models to predict stable helix shapes. Shown are the geometry, mesh and boundary conditions used for (a) introducing the pre-stress, and (b) obtaining helical shape configurations. Note: $U_{x,y,z}$, and $R_{x,y,z}$ refer to displacement and rotational degrees-of-freedom respectively.

Following the pre-stress process, the model was updated into the ladder configuration by joining both (now stressed) composite strips with connectors. The deformed shape of the strips was imported as an orphan mesh, and the stress state was applied using an *initial state* predefined field. Ten RPs were placed midway between the two flanges and equally spaced along their length. These act as the midpoint of the spokes, and are later used to apply boundary conditions to the model, as shown in Figure 4(b). The RPs were then connected to each flange using *join + revolute* type connectors, which result in a rigid connection between the flanges with only rotations about the connector axis being permitted. At this stage, the model could be manipulated (using different boundary conditions) into a regular helix configuration (with a constant angle θ) or into a helix featuring a perversion (with a transition from a positive to a negative angle θ).

Helix shape configuration

Obtaining the $\theta = 45^{\circ}$ configuration of the manufactured demonstrator involved adding a rotational boundary condition to perturb the structure. Rotational boundary conditions could then be applied to RP10 (6.28 rad) and RP1 (-5 rad) in the first step. Removing these rotations in the subsequent step resulted in the structure continuing to deform into the helical shape configuration.

During the deformation process, it was noted that the flange regions between the spokes are subject to local buckling. Due to the quasi-static nature of the model, these areas required artificial damping (through the use of the ABAQUS function *Automatic Stabilization*) to aid in obtaining a converged solution. For this analysis, an energy fraction of 1×10^{-4} N s mm^{-1} was required in the first step only. The value of the stabilisation factor used must be kept at a minimum, otherwise the accuracy of the

solution may be affected.

Helix featuring a perversion

To obtain a local reversal in twist direction, two analyses were conducted. First, as per the analytical model presented by Lessinnes and Goriely[9], the distance between the flanges was restricted by maintaining the spoke count in the area of the perversion. This model is subsequently referred to as the 'constrained' model. Rotations of 5.5 rad and 4.4 rad were applied to RP1 and RP10 respectively. These were then removed in the second step, and the structure continued to deform into two separate helical shapes of opposing angle θ. As before, artificial damping was required, with 1 x 10^{-7} N s mm^{-1} and 5 x 10^{-6} N s mm^{-1} being used in the first and second steps, respectively.

A second perversion configuration was modelled to match the experimentally observed geometry. In this case, the middle spoke (RP5) was eliminated. This permitted the distance between the flanges to change during the formation of the perversion, and so this model is referred to as the 'unconstrained' model. The boundary conditions applied were as in Figure 4 (b), with the nodes at the centre of the flanges being restricted in both *x*- and *y*-axis displacements. This eliminates rigid body motion, while still allowing the flanges to rotate about the *x*-axis.

Before applying rotations, the distance between the flanges at the location of the missing spoke was increased by adding a displacement. This was necessary to 'coax' the solution to the desired perversion shape. Rotations of 5.5 rads and 4.4 rads were then applied to RP10 and RP1. In this case, damping factors of 5 x 10^{-5} N s mm^{-1} and 3 x 10^{-5} N s mm^{-1} were required in the second (twisting) and third steps, respectively. The three shape configurations obtained from FE models are shown in Figure 5.

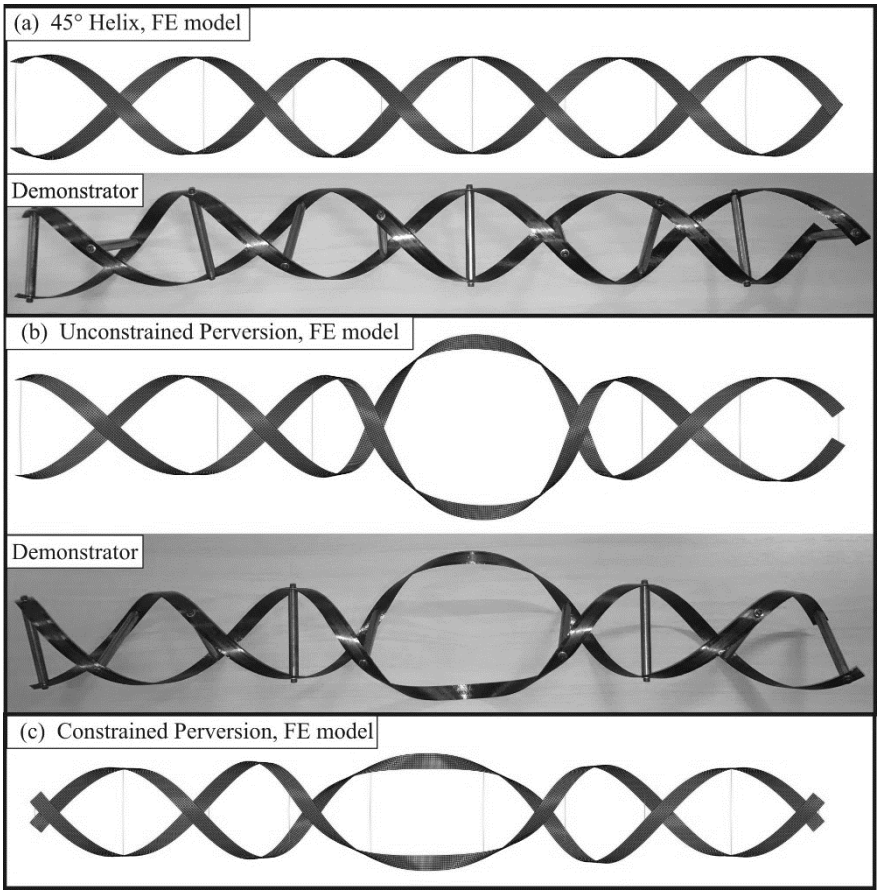

Figure 5: Equilibrium shape configurations from FE models, showing (a) helix configuration; (b) unconstrained perversion configuration; and (c) constrained perversion configuration. The experimentally observed shapes for the helix and unconstrained perversion are provided for comparison.

3.2 FE Model to monitor strain energy development

Having correctly predicted the experimentally observed shape configurations, the FE model was then used to gain insight into why the constrained perversion was not obtainable in practice. This required some modifications to the model presented in Section 3.1. To facilitate continuous monitoring of the strain energy formation during deformation, a single analysis was used for both the pre-stressing and deformation phases. As the connectors cannot be modified in a single analysis, only one strip was modelled. This is possible due to the symmetry of the structure, and uses the same model configuration as shown in Figure 4(a) The prestress and subsequent deformation into a helix could then be controlled through boundary conditions imposed at the RPs, as per the model in Section 3.1.

The onset of failure observed in the demonstrator indicated the formation of large strains. Indeed, monitoring the strain energy developed during deformation verifies this point. Figure 6 shows the strain energy developed for the three shape configurations. The plots start from the strain energy at the reference, ladder, shape configuration. As rotations are applied to the RPs, the structure is perturbed towards a state of low strain energy. It can be seen that the constrained perversion features the highest strain energy of all three configurations, with over three times the strain energy of the helix shape. Secondly, examining the strain energy at the beginning of the deformation shows that the strain energy increases in the constrained perversion case. Examining Eqn (1) below, this increase in energy required indicates that higher stresses and strains are formed as a result.

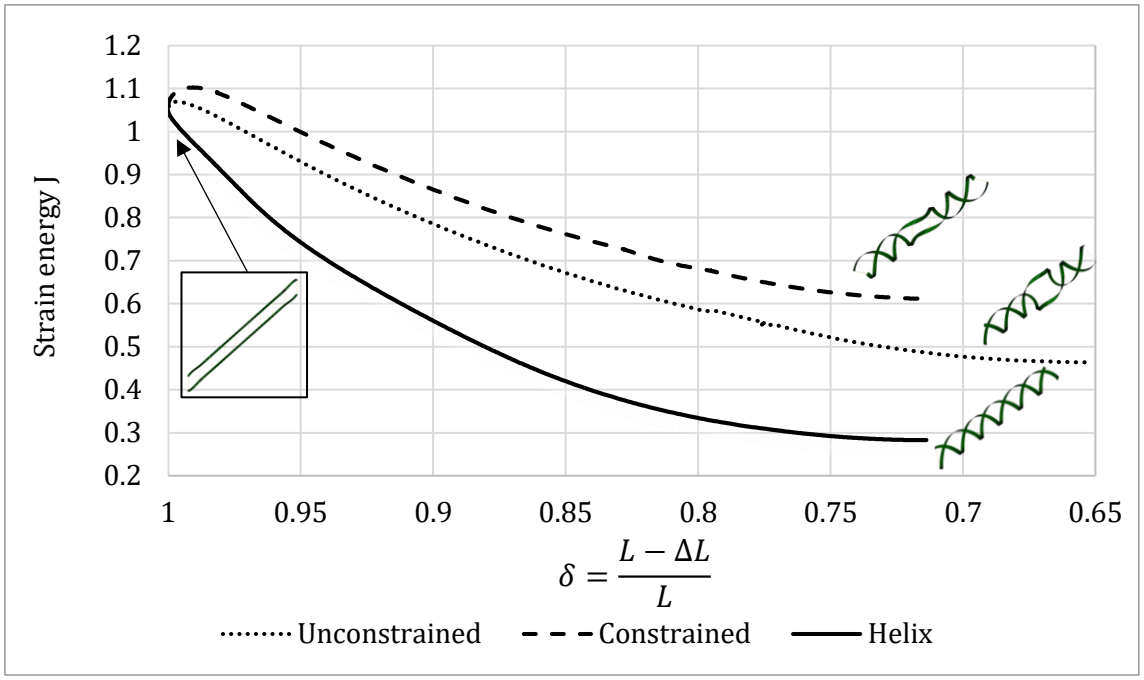

Figure 6: Strain energy formation of one strip of the helical structure, with and without perversions. Note: *ALLSE* history output was used to generate the plot.

3.3 Ratio of membrane to flexural strains

It was shown in section 3.1 that the constrained perversion shape features an increase in strain energy, which could be a factor in that shape not being obtainable with the demonstrator. To further verify this point, the contribution of flexural (henceforth including both bending and twist) and membrane strains to the total strain energy were examined. To do so, the extensional strains and bending strains (*SE* and *SK* Abaqus outputs, respectively) were extracted. This was done at the final increment of the analysis (*i.e.* for the stable shape configurations). The contribution of each component to the total strain energy could then be examined according to the following anaysis.
The general form of the strain energy (U) of the flanges is given by:

$$U = \frac{1}{2}\int_v \sigma^T \varepsilon \, dv \tag{1}$$

Applying Classical Laminate Plate Theory (CLPT), this expands to:

$$U = \frac{1}{2}\int_{-t/2}^{t/2}\int_\Omega \sigma_{xx}\varepsilon_{xx} + \sigma_{yy}\varepsilon_{yy} + \tau_{xy}\gamma_{xy}\, d\Omega\, dz \tag{2}$$

where σ_{ij}, ε_{ij}, τ_{ij}, and γ_{ij} ($i, j = x,y$) are the laminate stresses, strains, shear stresses and shear strains, respectively, and t is the laminate thickness.

Integrating the stresses through the thickness, the force (N) and moment (M) resultants can now be introduced:

$$U = \frac{1}{2}\int_\Omega N_x\varepsilon^0_{xx} + N_y\varepsilon^0_{yy} + N_{xy}\gamma^0_{xy} + M_x k^0_x + M_y k^0_y + M_{xy}k^0_{xy}\, d\Omega \tag{3}$$

where k_{ij} ($i, j = x,y$) are principle curvatures, and the superscript '^{0}' denotes mid-plane values.
Considering the [0_4] lay-up of the flanges, the resultants take the form of:

$$\begin{aligned} N_x &= A_{11}\varepsilon_{xx}^0 + A_{12}\varepsilon_{yy}^0 \\ N_y &= A_{12}\varepsilon_{xx}^0 + A_{22}\varepsilon_{yy}^0 \\ N_{xy} &= A_{66}\gamma_{xy}^0 \\ M_x &= D_{11}k_x^0 + D_{12}k_y^0 \\ M_y &= D_{12}k_x^0 + D_{22}k_y^0 \\ M_{xy} &= D_{66}k_{xy}^0 \end{aligned} \tag{4}$$

The strain energy can then be written as:

$$U = \frac{1}{2}\int_{\Omega} A_{11}{\varepsilon_{xx}^0}^2 + A_{22}{\varepsilon_{yy}^0}^2 + 2A_{12}\varepsilon_{xx}^0\varepsilon_{yy}^0 + A_{66}{\gamma_{xy}^0}^2 + D_{11}{k_x^0}^2 + D_{22}{k_y^0}^2 + 2D_{12}k_x^0k_y^0 + D_{66}{k_{xy}^0}^2\, d\Omega \tag{5}$$

Finally, the membrane and flexural components to the strain energy (U_e and U_f, respectively) can be extracted:

$$U_e = \frac{1}{2}\int_{\Omega} A_{11}{\varepsilon_{xx}^0}^2 + A_{22}{\varepsilon_{yy}^0}^2 + 2A_{12}\varepsilon_{xx}^0\varepsilon_{yy}^0 + A_{66}{\gamma_{xy}^0}^2\, d\Omega \tag{6}$$

$$U_f = \frac{1}{2}\int_{\Omega} D_{11}{k_x^0}^2 + D_{22}{k_y^0}^2 + 2D_{12}k_x^0k_y^0 + D_{66}{k_{xy}^0}^2 d\Omega$$

Equation 6 is then evaluated for each element of the structure, providing the total membrane (U_e) and flexural (U_f) strain energy contributions. These are given in Table 2 for the ladder configuration and the three helix configurations.

	Strain Energy (mJ)				
	U_e Membrane	U_f Flexural	$\varphi = {U_e}/{U_f}$	Total $U_e + U_f$	Total (Abaqus)
Ladder	0.2317	1061.9	0.00022	1062.2	1062.1
Helix	7	272.6	0.0256	279.6	282.3
Constrained Helix	31.5	559.1	0.0564	590.7	610.8
Unconstrained Helix	12.1	445.0	0.0272	457.1	463.6

Table 2: Membrane and flexural strain contributions U_e and U_f to total strain energy state at equilibrium shape configurations.

From Table 2 it can be seen that the ratio of membrane to flexural strain energy in the ladder configuration was very small at φ = 0.00022. This is due to the fact that the flanges were simply flattened from a coiled to a flat state, inducing only flexural strains, with very limited mid-plane stretching occurring. Moving to the helix shape configuration, there is still a small magnitude of mid-plane strains occurring, which thus keeps φ low. When considering the perversion states, however, the membrane strains developed become higher. Compared to 7 mJ for the helix, U_e increased to 12.1 and 31.5 mJ for the unconstrained and constrained perversion shapes, respectively. This increase in membrane strain energy leads to two interesting observations. Firstly, as flexural strains are capable of producing large deformations, they are particularly suited to morphing structures that require large changes in shape. The small ratio of φ of the helix shape demonstrates how optimised the shape is to morphing configurations, as the majority of strain energy is obtained through flexural strains, thus resulting in very large deformations being possible. Secondly, as has been previously noted, the increases in strain energy

is directly related to an increase in strains (see Eqn. (1)). The constrained perversion required an increase in strain energy from that of the ladder configuration. This indicates that the strains may become too large to develop this configuration without material failure. This effect is further exacerbated by the stress increases in the area of the bolt holes in the flanges which are used to attach the spokes.

Note that the difference in total between the summation of bending and flexural strain energies and the total outputted from Abaqus (final column in Table 2) is due to other contributions which were not considered in this study (*e.g.* transverse shear strains).

4 DISCUSSION

The morphing helix is a versatile morphing structure capable of existing in a number of stable shape configurations. Manufacturing the structure from composite materials provides an exceptionally lightweight and yet stiff structure. In addition, the negligible mid-plane strains developed demonstrate the efficiency of the morphing helix as a shape changing structure. The internal strains developed are a result of bending, from which large shape changes are possible. It is therefore an elegant solution to the problem facing morphing structures (obtaining a light weight, compliant, and yet stiff structure). Adding local twist perversions to the structure drastically increases the versatility of the structure, as the morphing combinations can potentially become limitless. Should it be possible to control the length and number of perversions introduced into a helix, then discrete sections of the helix may be treated as modular morphing sections, with each one being deployed individually. Combined with the rich tunability possible with the morphing helix, this results in a highly flexible and morphing structure with exceptional morphing combinations. The flexibility added by the perversion extends beyond additional shape configurations being possible. The local changes in geometry also changes the structural response of the system. For example, by creating a perversion, the vibrational or load-displacement response of the structure can be changed. This opens a new category of morphing structures for development.

The use of AFP to manufacture the flanges of this structure adds significantly to the viability of the technology. The process offers a significant reduction in manufacturing time and complexity when compared to traditional autoclave techniques. More excitingly, the potential to steer the fibre direction can lead to drastically different morphing concepts to be developed, with further morphing combinations being possible.

This work has shed light on the mechanical behaviour of the flanges when introducing a perversion. The strains developed by introducing a perversion may be prohibitively high, in particular when bolt holes are included in the flanges. It must be noted however that the conditions specified by Lessinnes and Goriely [9] to introduce a perversion were not strictly followed, and thus a different perversion type (with less severe stains) may be possible. In this instance, removing the boundary condition imposed by a spoke adequately relaxed the development of strains, allowing for the perversion to form. Bearing this in mind, further investigations into the strain energy formation is planned. However, the current findings do highlight that previous assumptions neglecting membrane strains may need modification in theoretical models.

This knowledge will then be used to use perversions to create novel morphing concepts. In the longer term, the controllability of the perversion needs to be determined. Specifically, the limitations to the number and size of perversions that can be introduced into a structure are currently unknown. Likewise, suitable activation systems need to be developed to control this behaviour.

5 CONCLUSIONS

A multistable helix structure is presented, featuring a new twist reversing shape perversion. Multistability is achieved by flattening and connecting two initially curved composite strips, introducing strain energy. The composite flanges were manufactured using automated fibre placement, resulting in a reduction in manufacturing time and complexity. Following manufacture, the structure was capable of achieving a ±45° twist angle. In addition, it was possible to obtainable a perversion in the structure, but this required the removal of a connecting spoke to alleviate high strains. Finite element analysis of the helix with constrained and unconstrained perversions showed high levels of strain energy (and thus strains) being developed in the constrained perversion case. These high strains indicate that the constrained perversion may not be obtainable before material failure. In addition, the assumption used

in theoretical models which neglects extensional strains was verified when consider regular helix shapes only. Therefore, their inclusion into theoretical models may be required to correctly predict the behaviour of helices with perversions. Future work aims to further characterise the perversion configurations, with a goal towards implementing them into morphing structures.

ACKNOWLEDGEMENTS

This work has been undertaken under the Varicomp Projects with funding from Science Foundation Ireland under its Research Professor scheme.

REFERENCES

1. Lachenal, X., S. Daynes, and P.M. Weaver, *Review of morphing concepts and materials for wind turbine blade applications.* Wind Energy, 2013. **16**(2): p. 283-307.
2. Daynes, S. and P.M. Weaver, *A morphing trailing edge device for a wind turbine.* Journal of Intelligent Material Systems and Structures, 2012. **23**(6): p. 691-701.
3. Scott, S., et al., *Gust response of aeroelastically tailored wind turbines.* Journal of Physics: Conference Series, 2016. **753**: p. 042006.
4. Lachenal, X., P.M. Weaver, and S. Daynes, *Multi-stable composite twisting structure for morphing applications.* Proceedings of the Royal Society A: Mathematical, Physical and Engineering Sciences, 2012. **468**(2141): p. 1230-1251.
5. Puig, L., A. Barton, and N. Rando, *A review on large deployable structures for astrophysics missions.* Acta Astronautica, 2010. **67**(1–2): p. 12-26.
6. Ursache, N.M., A.J. Keane, and N.W. Bressloff, *Design of Postbuckled Spinal Structures for Airfoil Camber and Shape Control.* AIAA Journal, 2006. **44**(12): p. 3115-3124.
7. Davis, L.P., et al., *The application of thermally induced multistable composites to morphing aircraft structures.* 2008. **6930**: p. 693012.
8. Schultz, M.R., *A Concept for Airfoil-like Active Bistable Twisting Structures.* Journal of Intelligent Material Systems and Structures, 2008. **19**(2): p. 157-169.
9. Lessinnes, T. and A. Goriely, *Design and stability of a family of deployable structures.* Preprint: http://arxiv.org/abs/1604.07014v1, 2016.